Journal of the Physical Society of Japan **92**, 121010 (2023)
https://doi.org/10.7566/JPSJ.92.121010

Designing Shape Transitions in Elastic Structures

Basile Radisson and Eva Kanso

Department of Aerospace and Mechanical Engineering, University of Southern California, Los Angeles, CA 90089-1191, U.S.A.

(Received August 1, 2023; accepted September 11, 2023; published online November 21, 2023)

Many biological and engineered systems, from the Venus flytrap to mechanical metamaterials, exploit elastic instabilities and snap-through transitions to achieve a targeted function. Elastic strips, that buckle into one of two stable equilibrium states and snap from one state to the other as that state becomes unstable or suddenly disappears, have emerged as canonical systems for analyzing shape transitions. Here, we review recent advances that explain how geometric symmetries and symmetry-breaking mechanisms govern shape transitions in boundary-actuated elastic strips and provide universal rules for predicting or designing such transitions. We highlight the opportunities that this geometric understanding offers to emerging research areas, such as multi-functional metamaterials, morphological computing, and mechanical intelligence.

1. Introduction

An elastic strip of length L, whose ends are first brought together by a distance ΔL to cause the strip to buckle into one of two stable shapes, provides an intuitive system to demonstrate shape transitions. The buckled strip is bistable, with two stable equilibrium states that, energetically, occupy two equally-deep potential wells (Fig. 1). Snap through occurs when the strip is in one equilibrium state that becomes unstable or suddenly disappears as a control parameter is varied. This snap through is accompanied by a rapid release of stored elastic energy and is used as a motif for energy transfer in many biological and engineered systems; examples range from the familiar Venus flytrap[1)] and hopper popper toys[2)] to jumping robots[3)] and unconventional mechanical metamaterials.[4–6)]

In the carnivorous Venus flytrap example, mechanosensing and snap-through instabilities are combined in a remarkable way to produce biological function, namely, prey capture. Mechanosensitive hairs lining the inner surface of the flytrap leaf deflect and generate electrical signals (action potential spikes) when a landed prey touches them. To avoid false or not fully landed prey, the flytrap requires two consecutive action potentials within 30 s to initiate a stereotypical response to close its lobes: two consecutive signals trigger a hydraulically driven lobe deformation, which onsets a fast trap closure in about 100 ms. This fast closure — the fastest motion in the plant kingdom — results from a snap-through buckling instability.[1)]

Snap-through transitions have been instrumental in the design of metamaterials made of multistable building blocks. Transitions at the individual block level allow for the emergence of impressive properties at the material level, such as non-reciprocal propagation of elastic waves,[6)] or non-linear and programmable stress-strain responses.[4)] The metamaterial properties can be finely controlled by tuning the energy landscape of the constitutive blocks.[6)] It is thus important to understand the mechanisms leading to shape transitions in an elastic strip, both as an elementary actuator in robotic systems[3)] and multi-functional metamaterials[4–6)] and as a canonical example of bifurcation theory in infinite-dimensional continua.[7,8)]

Here, we present a focused review of snap-through transitions in buckled elastic strips actuated at their boundaries based on the results in Refs. 9–12. The broader dynamics of elastic filaments and strips has been and continues to be extensively treated in the literature — see, e.g., Refs. 7, 8, 13, and 14 and references therein — and is beyond the scope of the present review.

The Euler-buckled strip admits, in addition to the two fundamental stable U-shape equilibria, denoted U_A and U_B in Fig. 1, an infinite family of unstable equilibria that come in pairs, ordered by increasing value of elastic bending energy. We refer to members of the same pair, including the fundamental U-shaped pair, as *twin solutions*. The first unstable solution consists of a pair of S-shape equilibria labeled S_A and S_B. In Fig. 1, we unfold the energy landscape and represent it schematically in a one-dimensional form. This reduced representation highlights the minimum energy barrier — energetic difference in $\mathcal{E}_b$ between $S_{A,B}$ and $U_{A,B}$ — that the strip needs to overcome in order to undergo a shape transition from U_A to U_B.

A buckled strip can be forced to snap from one equilibrium state to another by applying a transverse force F_{ext} at the midpoint of the buckled strip.[2)] This method for controlling the snap-through instability is commonly employed in micro-electromechanical switches,[15)] insect-inspired jumping robots,[3)] and mechanical metamaterials.[6)]

Snap-through can also be triggered by boundary actuation, which is the main focus of this review. For example, snap-through was demonstrated in a clamped-hinged strip with the hinged end free to rotate in place and the clamped end sheared by a distance d in the direction transverse to the buckled strip[10)] (Fig. 2). Similar boundary actuation with both ends clamped led to graceful merging of the two equilibrium states.[10)] Yet, in a previous study, when both ends of a clamped–clamped strip were rotated symmetrically, the strip snapped from one equilibrium to another[9)] (Fig. 3). Snap-through was also observed when only one end was rotated. That is, both symmetric and asymmetric boundary rotations led to snap-through transitions, but the character of the snapping differed depending on the boundary conditions. Specifically, in the case of symmetric boundary rotations, the early snap-through dynamics is linear, and the typical distance between the strip's actual configuration and its initial configuration grows exponentially in time, thus the term *exponential snap-through*; in the asymmetric case, the strip moves away from its initial configuration in an algebraic manner, thus called *algebraic snap-through*.

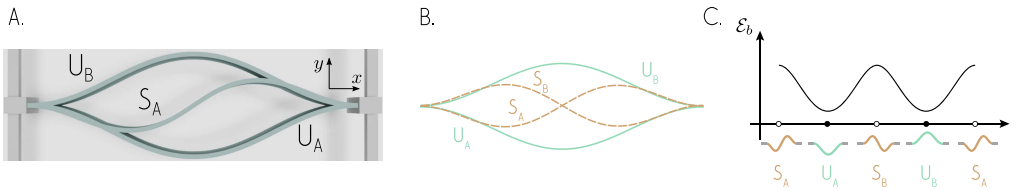

Fig. 1. (Color online) Buckled elastic beam (A) 3D rendering of buckled elastic beams obtained through numerical simulations based on the 3D Cosserat equations with $L/\Delta L = 20$. (B) Plot of the two stable equilibria U_A and U_B and two unstable equilibria of lowest bending energy S_A and S_B obtained from the analysis of the stationary quasi-linear beam model with $L/\Delta L = 20$. (C) Schematic of the simplified energy landscape of the Euler buckled beam. The energy landscape is represented here on a one-dimensional periodic space, depicting two potential wells at the two stable equilibria $U_{A,B}$ separated by lowest energy barriers at the first pair of unstable equilibria $S_{A,B}$. The beam can pass from U_A to U_B (or vice versa) by passing through either S_A or S_B.

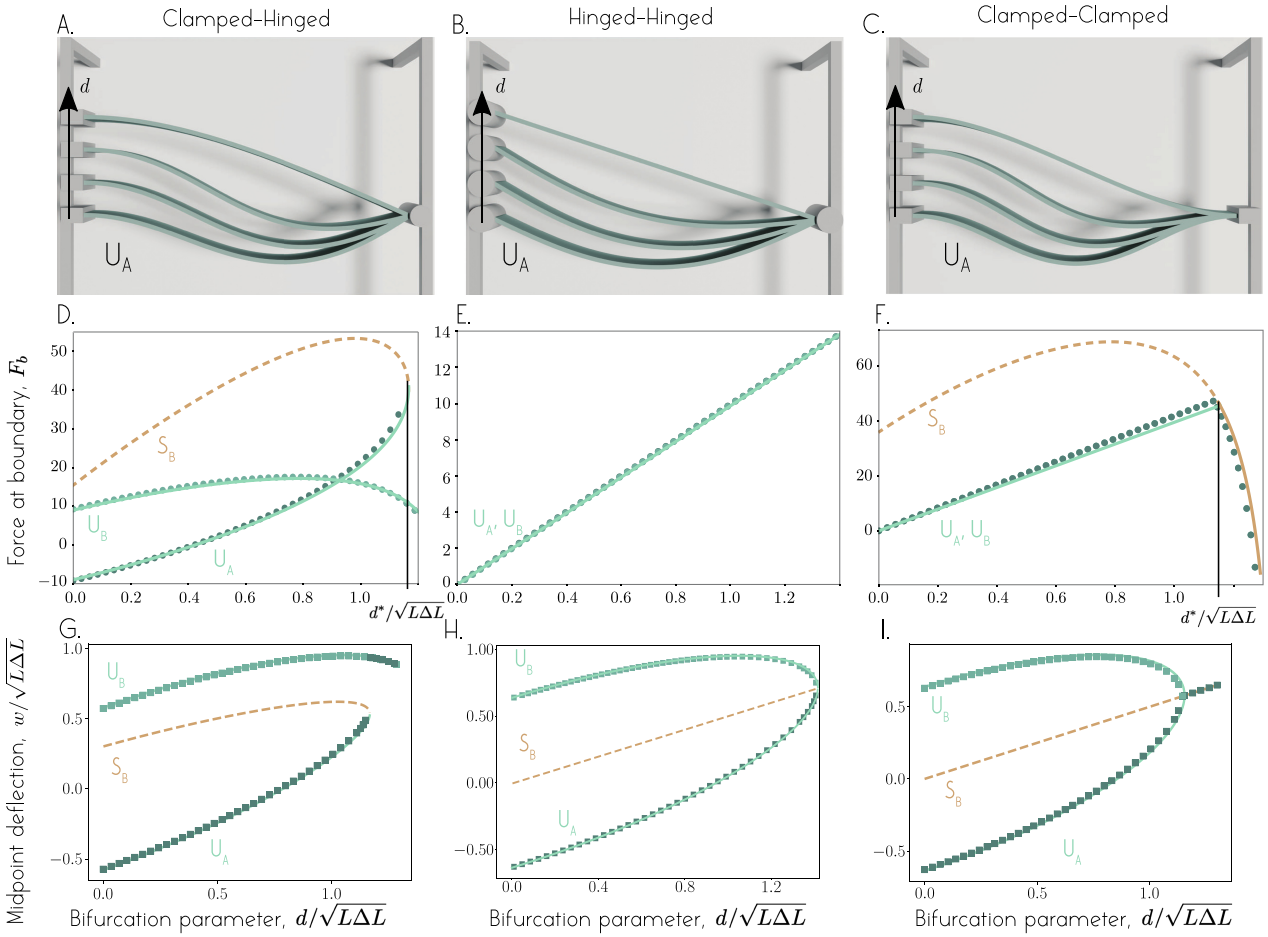

Fig. 2. (Color online) Equilibrium configurations of the Euler-buckled strip under transverse shearing of the boundaries. Starting from the equilibrium shapes $U_{A,B}$ of the Euler-buckled, these equilibria morph into different shapes as as a misalignment d is introduced between the two boundaries. (A)–(C) Evolution of the U_A configuration for different d values for the clamped–clamped, hinged–hinged, and clamped-hinged boundary conditions. (D)–(F) Evolution of the non-dimensional transverse force applied on the left clamped boundary of the strip under translational actuation in terms of the non-dimensional bifurcation parameter $\mu = d/\sqrt{L\Delta L}$. The force is obtained analytically from the Euler beam model (full line) and numerically from the discrete Cosserat equations (symbols). (G)–(I) Evolution of the non-dimensional midpoint deflection of the strip as a function of the non-dimensional misalignment parameter μ_d. The green symbols represent data from numerical Cosserat simulations and the lines data from the Euler beam analysis (full lines for stable equilibrium and dashed lines for unstable ones).

A deeper understanding of the mechanisms that dictate the type of shape transition, algebraic or exponential snap-though or graceful merging of equilibria, remained lacking until recently.[11,12] In Refs. 11 and 12, we extended the mathematical analysis of Ref. 9 to reveal the mechanisms governing shape transitions in boundary-actuated elastic strips, and we showed that the two systems in Refs. 9 and 10 are equivalent. Importantly, to predict the type of bifurcation and establish design rules for creating a desired shape transition, we showed that these transitions are governed by geometric symmetries. Here, we review and summarize these findings.

2. Shape Transitions in Boundary-Actuated Buckled Elastic Strips

In this section, we review recent experimental and mathematical studies of shape transitions in elastic strips. This review focuses on the violent and gentle shape transitions reported in Refs. 9–12.

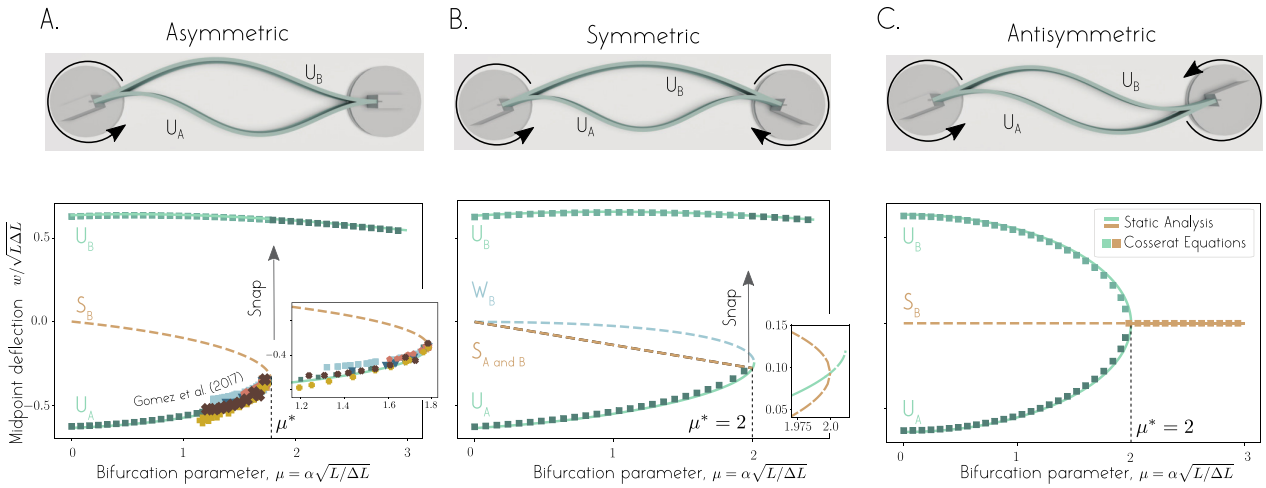

Fig. 3. (Color online) Equilibrium configurations of the Euler-buckled strip under rotational actuation. One or both ends of the clamped–clamped strip are (quasi-statically) rotated by an angle α, leading to loss of bistability as α increases. (A) Asymmetric actuation (one end is rotated) and (B) symmetric actuation (both ends are rotated by the same amount in opposite direction) lead to violent snap-through. (C) Antisymmetric actuation (both ends are rotated by the same amount in the same direction) leads to a smooth transition. Midpoint deflection of the strip as a function of the bifurcation parameter $\mu = \alpha\sqrt{L/\Delta L}$. Green squares represent data obtained from numerical simulations based on the Cosserat rod theory. Solid and dashed lines represent, respectively, stable and unstable branches obtained from the static analysis of the Euler beam model. Colored markers represent experimental data from Ref. 9.

2.1 *Transverse boundary actuation*

Sano and Wada[10] considered a clamped-hinged buckled strip that is actuated by applying a misalignment d between its two ends [Fig. 2(A)]. In their experiment, they observed, at a threshold value of the control parameter $d = d^*$, a snap-through transition where the beam suddenly snapped from U_A to U_B. They measured the vertical force F_b applied by the strip on the left clamped boundary. At $d = d^*$, as the beam suddenly snapped, they observed a sudden drop in force F_b. Decreasing d after snap-through, they showed a strong hysteresis in the measured force depending on the configuration U_A or U_B of the strip. These observations were corroborated by theoretical and numerical analysis that showed that the system suddenly passes from a bistable to monostable configuration at $d = d^*$. Importantly, they showed that the force hysteresis obtained in the clamped-hinged strip did not occur in clamped–clamped and hinged–hinged strips. The authors attributed this hysteresis to be a consequence of the asymmetry between the two boundary conditions.

In Refs. 11 and 12, we investigated the bifurcation behavior of the three systems introduced in Ref. 10 numerically, by leveraging the three-dimensional (3D) Cosserat theory, and its discrete counterpart, the discrete elastic rod [see (Ref. 11, Supplemental document)]. To establish bifurcation diagrams and carry out asymptotic analysis, we also analyzed the strip's behavior in the limit of small deflection $w(x, t)$, with $-L/2 < x < L/2$, based on the Euler-Bernoulli Beam theory [see (Ref. 11, Supplemental document)],

$$\rho bh\frac{\partial^2 w}{\partial t^2} + B\frac{\partial^4 w}{\partial x^4} + F\frac{\partial^2 w}{\partial x^2} = 0. \tag{1}$$

The material properties of the strip are denoted by ρ (density), b (width), h (thickness), and $B = Ebh^3/12$ (bending stiffness, with E the Young's modulus). The applied compressive load is denoted by F. In this limit, the inextensibility condition gives rise to the nonlinear constraint equation

$$\int_{-L/2}^{L/2}\left(\frac{\partial w}{\partial x}\right)^2 dx = 2\Delta L. \tag{2}$$

Upon introducing the non-dimensional quantities,[9]

$$W = \frac{w}{\sqrt{L\Delta L}}, \quad X = \frac{x}{L}, \quad T = \sqrt{\frac{B}{\rho bhL^4}}t, \quad \Lambda^2 = \frac{FL^2}{B}, \tag{3}$$

we represented the configuration of the beam by the non dimensional transverse deflection of the beam $W(X, T)$ at non-dimensional abscissa X $(-1/2 < X < 1/2)$ and non-dimensional time instant T. The non-dimensional longitudinal compression force is $\Lambda^2 = FL^2/B$.

In Fig. 2, we show results from our numerical and theoretical analysis of the three systems introduced in Ref. 10 and analyzed in Ref. 11. Figures 2(A)–2(C) show a 3D rendering of the equilibrium configurations obtained by numerically solving the non-linear Cosserat equations.

In Figs. 2(D)–2(F), we report the non-dimensional force F_b calculated at the boundary in our numerical simulations of the Cosserat rod model (green symbols) along with the force obtained from our theoretical analysis (4) (solid and dashed lines). These results corroborate the findings of Sano and Wada:[10] the force F_b shows a strong hysteresis in the case of clamped-hinged boundary conditions [Fig. 2(D)] that is not observed in the hinged–hinged and clamped–clamped boundary conditions [Figs. 2(E) and 2(F)].

To shed light on the force hysteresis in the clamped-hinged case in Fig. 2(D), it is instructive to reproduce the explicit expressions for F_b that we derived based on the quasi-linear Euler beam model,

$$\text{clamped-hinged:} \quad F_b = \frac{d}{\sqrt{L\Delta L}}\frac{\Lambda^3\cos\Lambda}{\Lambda\cos\Lambda - \sin\Lambda}, \tag{4}$$
$$\text{hinged–hinged and clamped–clamped:} \quad F_b = \frac{d}{\sqrt{L\Delta L}}\Lambda^2.$$

In all cases, the expression for F_b is the same for both equilibria U_A and U_B. However, in the clamped-hinged case, the value of Λ, which depends on the shape of the strip, differs between these equilibria, because, as soon as $d \neq 0$, U_A

and U_B are no longer energetically equivalent. In contrast, in the clamped–clamped and hinged–hinged configurations, the two equilibria are energetically identical. These observations can be verified analytically, using the explicit form of the equilibria (Ref. 11, Supplemental document), or geometrically, by viewing the two configurations $U_{A,B}$ in an orthonormal frame of reference, with one axis connecting the two end points of the strip. Geometric symmetry in the clamped–clamped and hinged–hinged cases is evident in such reference frame, but is broken in the clamped-hinged case. These geometric symmetries between U_A and U_B solutions play an important role, not only in the force hysterisis, but also in the bifurcations that the system undergoes; symmetry breaking is discussed at length in Sect. 4.

In Figs. 2(G)–2(I), we show the evolution of the non-dimensional midpoint deflection $w_0/\sqrt{L\Delta L}$ of the equilibria obtained from our numerical simulations and from our analytical calculations in term of the non-dimensional control parameter $d/\sqrt{L\Delta L}$. Stable equilibria are shown as full lines while unstable ones are plotted as dashed lines. These results show that the violent transition observed at $d = d^*$ in the case of clamped-hinged boundaries results from one stable and one unstable equilibria that merge and suddenly disappear. This is the hallmark of a *saddle-node bifurcation*.

In the clamped–clamped and hinged–hinged cases, a transition from bistable to monostable is observed at a threshold value of the control parameter, but these transitions are characterized by a smooth merging between two stable and one unstable equilibrium branches. This is the hallmark of a supercritical *pitchfork bifurcation*.

2.2 *Rotational boundary actuation*

Gomez et al.[9] considered a clamped–clamped buckled strip that is actuated by rotating one or both of its boundaries by an angle α (Fig. 3). In their experiment, the strip was initially in one, say U_A, of the two buckled stable states with angle $\alpha = 0$ at both boundaries. The angle imposed at the left boundary was then quasi-statically increased by small increments while the other end of the beam remained fixed [Fig. 3(A)]. As the angle α reached a threshold value α^*, the authors observed a violent snap-through transition where the strip suddenly jumped to U_B.

In Fig. 3, we show results from our numerical and theoretical analysis of the two systems introduced in Ref. 9 with asymmetric and symmetric boundary actuation and a third system of antisymmetric actuation.[11,12]

Figure 3(B) shows the evolution of the non-dimensional midpoint deflection $w_0/\sqrt{L\Delta L}$ in term of the non-dimensional angle $\mu = \alpha\sqrt{L/\Delta L}$ imposed at the left boundary. Colored markers show the experimental data obtained in Ref. 9, green markers show data obtained from Cosserat simulations and lines show theoretical results obtained from the analysis of the static quasi-linear beam model.[11,12] Experimental and numerical data show the same behavior: the strip jumps from U_A to U_B at $\mu = \mu^*$. Theoretical analysis shows that this snap-through transition occurs at a bifurcation where a stable branch (U_A) and an unstable one (S_B) merge and disappear.

Besides the asymmetric actuation analyzed in Ref. 9, we considered the case where both boundaries are rotated symmetrically [Fig. 3(B)] and antisymmetrically [Fig. 3(C)]. Numerical Cosserat simulations show that symmetric and antisymmetric actuations lead to a transition from a bistable to a monostable state at a bifurcation point $\mu = \mu^*$. In the symmetric case, for $\mu > \mu^*$, the beam snaps from U_A to U_B and the early dynamic is exponential.[9,12] Static and stability analysis of the quasi-linear beam model shows that snap-through occurs at a bifurcation where two unstable branches S_A and S_B merge with a stable branch U_A that becomes unstable [inset Fig. 3(B)].[9,11] This indicates a *subcritical pitchfork bifurcation*.

In the antisymmetric case, there is no snap-through, the two stable equilibrium branches U_A and U_B merge smoothly onto an unstable branch S_B at $\mu = \mu^*$. The latter becomes the only stable equilibrium for larger values of μ. These diagrams point to a *supercritical pitchfork bifurcation*.

The bifurcation diagram in Fig. 3(A) resembles the one in Fig. 2(G) for the clamped-hinged system under translational shearing of the strip's boundaries. Similarly, the bifurcation diagram in Fig. 3(C) resembles the bifurcation diagram in Fig. 2(I). This resemblance is not a coincidence. The two systems can be mapped to one-another by a clever choice of frame of reference [Fig. 4 and (Ref. 11, Supplemental document)]. That is, the distinct set-ups introduced in Refs. 10 and 9 are analogous.

3. Normal Forms Near Shape Transitions

In Refs. 11 and 12, we analyzed the solution branches that split off at the bifurcation point and the behavior of these solutions in the neighborhood of the bifurcation by deriving equations of the temporal evolution of the amplitudes of *critical normal modes*. By definition, the critical normal modes have eigenfrequencies that vanish at the bifurcation and are characterized by mildly unstable or slightly damped behavior near the bifurcation. All other modes are strongly damped and thus play a marginal role in the dynamics near the bifurcation. Normal forms are dynamic equations that describe the time evolution of the amplitude of the critical modes.[9,11,12] Importantly, the type of bifurcation exhibited by these normal forms provides a precise classification of the bifurcation underlying elastic shape transitions.

The derivation of the normal forms entails the introduction of a parameter $\Delta\mu = \mu - \mu^*$ that characterizes the distance to the bifurcation point in parameter space, and carrying out an asymptotic analysis in the limit $\Delta\mu \ll 1$. The details of this analysis are beyond the scope of the present review and can be found in (Refs. 9 and 11, Supplemental documents) and in Ref. 12. Here, we present a summary of the main findings.

Specifically, we review the normal modes for the three types of rotational boundary actuation. We let $A(T)\Phi(X)$ denote the leading order term in the asymptotic expansion of $W(X,T) - W^*_{eq}(X)$, where $W^*_{eq}(X)$ is the shape of the beam at the bifurcation. The leading order term has the following interpretation. Near the transition ($\Delta\mu > 0$), the strip moves away from its equilibrium configuration at the bifurcation following the mode $\Phi(X)$ whose amplitude $A(T)$ grows according to a dynamical equation obtained by carrying out the detailed asymptotic analysis.

For the asymmetric rotation, the amplitude equation was first derived in Ref. 9 and takes the form

$$\frac{d^2A}{dT^2} = a_{1,\mathrm{asym}}\Delta\mu + a_{2,\mathrm{asym}}A^2, \tag{5}$$

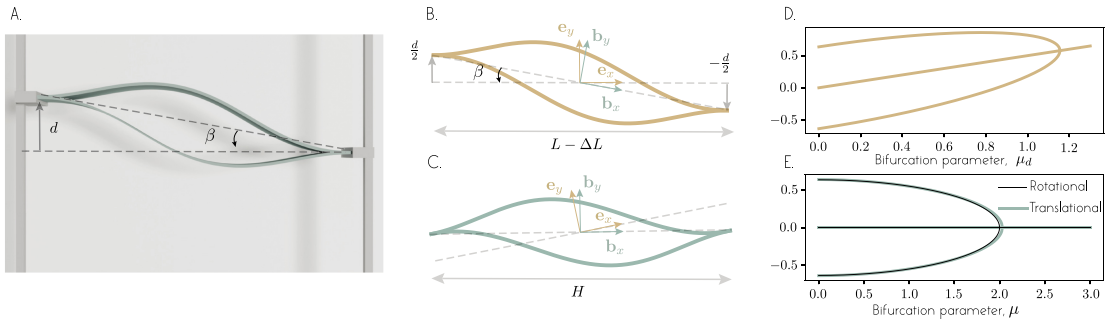

Fig. 4. (Color online) Change of frame of reference. The system with transverse boundary shearing in Fig. 2, when observed in a frame attached to the line that connects the two ends of the strip, becomes analogous to the system with rotational actuation depicted in Fig. 3. (A) 3D rendering of the two equilibria U_A and U_B from Fig. 2. (B) Corresponding analytical equilibria depicted in inertial frame $(\mathbf{e}_x, \mathbf{e}_y, \mathbf{e}_z)$. (C) Same equilibria depicted in the $(\mathbf{b}_x, \mathbf{b}_y, \mathbf{b}_z)$ Lagrangian frame where $\mathbf{b}_x$ is defined along the line that connects the two ends of the trip. (D) Bifurcation diagram obtained analytically for the transverse shearing case. (E) Comparison of the bifurcation diagram obtained for the transverse shearing case (green lines) and expressed in the Lagrangian frame $(\mathbf{b}_x, \mathbf{b}_y, \mathbf{b}_z)$ with the bifurcation diagram obtained for the case of antisymmetric rotational actuation (black lines). The two bifurcation diagrams align indicating that transverse shearing of the clamped–clamped beam in Fig. 2(C) is equivalent to the antisymmetric rotational actuation in Fig. 3(C). Similar argument can be made to show equivalence between the transverse shearing of the clamped-hinged beam in Fig. 2(A) with the asymmetric rotational actuation in Fig. 3(A).

where $a_{1,\text{asym}}$ and $a_{2,\text{asym}}$ are positive constants (explicit expressions in Ref. 9). The ODE (5) describes all the dynamic characteristics of the strip near the bifurcation point (Refs. 9 and 12). It has the normal form of a saddle-node bifurcation.[16] There is no linear term in (5) and thus no exponential growth. At early time, at small A, the snap-through dynamics is driven by the constant term and the dynamics is ballistic.

In Refs. 11 and 12, we extended the asymptotic analysis introduced in Ref. 9 to the cases of symmetric and antisymmetric actuation [Figs. 3(B) and 3(C)]. The reduced form that governs the evolution of the amplitude $A(T)$ of the leading order mode in the vicinity of the bifurcation point takes the form:

$$\frac{d^2A}{dT^2} = b_{1,(\cdot)}\Delta\mu A + b_{2,(\cdot)}A^3. \tag{6}$$

In the symmetric case, $b_{1,\text{sym}}$ and $b_{2,\text{sym}}$ are positive constants (full expression in Ref. 12) and (6) corresponds to the normal form of a subcritical pitchfork bifurcation. For $\Delta\mu > 0$, (6) admits only one unstable equilibrium (corresponding to U_A here[12]) and the beam snaps to the distant equilibrium U_B [not captured by the reduced form (6)]. The dynamics of this snap-through follows (6): at early time, the first term in (6) dominates and the dynamics is linear, as predicted in Ref. 9 and proven in Ref. 12; at later times, the destabilizing cubic term comes into play and A blows up to infinity. In reality, higher order non-linear terms come into play and saturate A when the beam reaches the new equilibrium U_B. This snap through differs from the snap-through dynamics observed in the asymmetric case [Fig. 3(A)] in that the strip initially goes away from its configuration at the bifurcation in an exponential manner, as opposed to the algebraic growth observed in the saddle-node bifurcation.[9,12]

In the antisymmetric case, $b_{1,\text{antisym}}$ and $b_{2,\text{antisym}}$ are both negative constants (full expression in Ref. 12) and (6) corresponds to a supercritical pitchfork bifurcation. For $\Delta\mu < 0$, there are two stable equilibria (U_A and U_B) and one unstable one (S_B). At $\Delta\mu = 0$, the two stable branches collapse onto the unstable one which becomes stable for $\Delta\mu > 0$. This explains that in Fig. 3(C), the transition from U_A and U_B to S_B is smooth.

4. Symmetries and Symmetry-Breaking Mechanisms

These studies show that the behavior of an elastic structure near a shape transition is tightly related to the type of bifurcation the system undergoes at the transition.[9,11,12] If one knows the type of bifurcation a system is likely to undergo, one can predict the functional form of the reduced equations and therefore predict the dynamic characteristics of elastic structure near these bifurcations.[9,12] In the following, we review the geometric mechanisms that select these different bifurcation types.[11]

Pitchfork bifurcations are known to arise in systems that possess binary symmetries. This is reflected by the invariance of (6) under a transformation $A \to -A$ (left-right symmetry). It is well known in bifurcation theory, that when an asymmetry is introduced in (6), the bifurcation takes the form of a saddle-node; see, e.g., Ref. 16. In Ref. 11, we showed that a similar symmetry breaking mechanism is responsible for the selection of the type of elastic shape transition.

For example the clamped–clamped and hinged–hinged beams exhibit smooth shape transition under transverse actuation [Figs. 2(H) and 2(I)] similar to that observed in the antisymmetric rotational actuation. Breaking the symmetry between the two boundaries using a clamped-hinged beam leads to snap-through [Fig. 2(G)] that resemble the saddle-node bifurcation obtained for the asymmetric rotational actuation. In the same way, symmetric and antisymmetric rotational actuation leads to pitchfork bifurcations while breaking all sort of symmetries between the two boundaries with asymmetric actuation yields a saddle-node.

But if symmetry is responsible for the selection of these bifurcations, which symmetry matters in these Euler buckled beam? How are the three types of elastic shape transitions reviewed in Fig. 3 selected through breaking of these symmetries?

To answer these questions, we start by reviewing the important geometric symmetries in the initial buckled beam configuration ($\alpha = 0$, $d = 0$). As pictured in Fig. 5, there are four important equilibrium shapes involved in the shape transitions analyzed in this review: the two stable U-shape equilibria that correspond to the two potential wells and the two unstable S-shape equilibria that correspond to the two

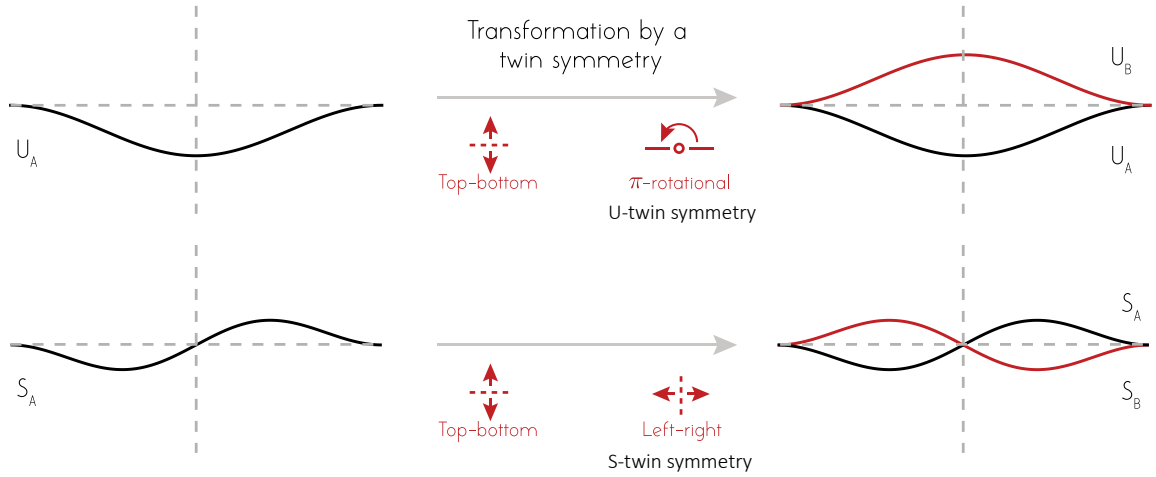

Fig. 5. (Color online) Euler buckling symmetries. Transformations that map a buckled configuration to its twin. We call the π-rotational symmetry that maps the U-shapes to one another the *U-twin symmetry* and the left-right symmetry that maps the S-shapes to one another the *S-twin symmetry*.

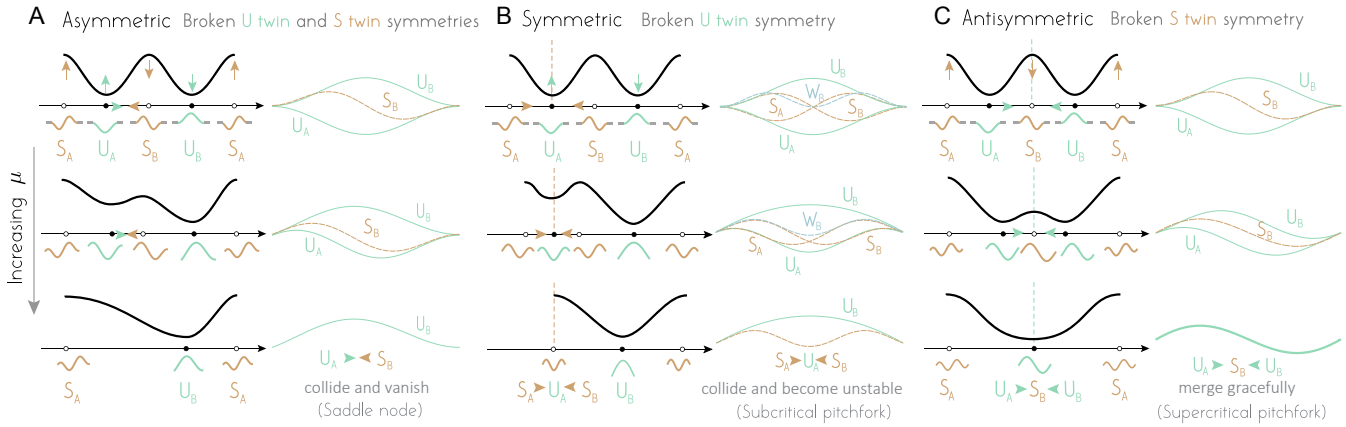

Fig. 6. (Color online) Potential energy landscape is intimately related to broken geometric symmetries that dictate the elastic shape transition. Energy landscape at $\mu = 0$ (top row, black lines) is characterized by two equally-deep potential wells at the two stable equilibria $U_{A,B}$ separated by lowest energy barriers at the first pair of unstable equilibria $S_{A,B}$. Rotating one or both of the boundaries reshapes the energy landscape: (A) breaking both U- and S-twin symmetries leads to a saddle-node bifurcation; (B, C) breaking either U- or S-twin symmetry leads to a pitchfork bifurcation. (B) In the symmetric case, the broken U-twin symmetry gives rise to a subcritical pitchfork bifurcation, where one of the stable equilibria, here U_A becomes unstable; the system must jump to U_B in a violent manner. Note that W_B denotes an unstable equilibrium at the next higher energy level compared to $S_{A,B}$ and its presence affects the dynamics of the snap-through as detailed in Ref. 12. (C) In the antisymmetric case, the broked S-twin symmetry gives rise to a supercritical pitchfork bifurcation, where both stable equilibria $U_{A,B}$ merge gracefully with the unstable equilibrium S_B, resulting in a single stable equilibrium.

lowest energy barriers [Fig. 1(B)]. Applying a transformation $w \to -w$ (top-bottom symmetry) to any of these shapes yields its twin configuration: it maps U_B to U_A and S_B to S_A, and vice-versa (Fig. 5). This symmetry is trivial because it is always broken under additional transverse shearing or rotational boundary actuation.

In addition to the trivial top-bottom symmetry, each of the U-shape and the S-shape equilibria admits a twin-symmetry which, when applied to that shape, yields its twin solution (Fig. 5). For the U-shape, the transformation $w \to -w$ $x \to -x$ maps U_B to U_A and vice-versa. We call this π-rotational symmetry the *U-twin symmetry*. For the S-shape, the transformation $x \to -x$ maps S_B to S_A and vice-versa. This left-right symmetry is called the *S twin symmetry*. These two twin symmetries govern the type of shape transition.

When the boundaries of the elastic beam are rotated [Figs. 1(A)–1(C)], the stable shapes U_A or U_B get deformed and the associated energy landscape shown in Fig. 1(B) is reshaped until one of the two potential wells (U_A or U_B) disappears. At this point, a shape transition is observed. The nature of this transition depends on whether the U twin symmetry and S twin symmetry are broken or conserved by the boundary actuation.[11] This is best seen by examining how the energy landscape gets deformed by the three types of rotational actuation (Fig. 6).

Both U- and S-twin symmetries get broken under asymmetric boundary actuation. Indeed, as shown in Fig. 6, asymmetric rotation at one end requires U_A to bend more than U_B and S_A to bend more than S_B, thus increasing the bending energy of U_A and S_A and decreasing that of U_B and S_B. This causes U_A and S_B to monotonically approach each other until they merge and suddenly vanish in a saddle node bifurcation. As U_A disappears, the system must jump to U_B in a snap-through transition.

The U-twin symmetry gets broken under symmetric actuation of both ends, but not the S-twin symmetry. The symmetric rotation of both ends requires U_A to bend more than U_B but it equally affects S_A and S_B. Thus, S_A and S_B remain energetically equivalent while the energy level of U_A increases and approaches that of S_A and S_B. Eventually, all

three equilibria, U_A, S_A, and S_B, all merge, giving rise to a single unstable equilibrium in a subcritical pitchfork bifurcation. As U_A becomes unstable, the system no option but to jump to U_B.

The S-twin symmetry gets broken under antisymmetric actuation, but not the U-twin symmetry. Here, U_A and U_B remain energetically equivalent while S_A bends more than S_B. For this antisymmetric actuation at the two ends, U_A and U_B monotonically approach S_B until they all gracefully merge in a single stable equilibrium in a supercritical pitchfork bifurcation. No snapping occurs.

This intuitive understanding of geometric symmetries and the role of symmetry-breaking is substantiated by the rigorous asymptotic analysis in Refs. 9, 11, and 12 and the resulting normal forms summarized in (5) and (6) near the shape transition.

5. Discussion

We presented a focused review of snap-through transitions in buckled elastic strips, with an emphasis on the role of symmetry and symmetry-breaking mechanisms in shaping these elastic transitions.

Symmetry is one of the most fundamental concepts in physics. It fashions the energy landscape and governs the equilibrium configurations the system can adopt. Broken symmetries are often invoked to explain transitions in physical systems, but bifurcation theory is typically explained using simple one-dimensional examples.[16] Extending this understanding to infinite-dimensional systems is challenging. The understanding we developed for elastic strips in Refs. 11 and 12 and reviewed here could serve as an educational tool to illustrate the role of symmetry-breaking in the bifurcation of infinite-dimensional continua. Importantly, snap-through transitions in boundary-actuated elastic strips result from one of two symmetry breaking mechanisms: one that causes a stable equilibrium to collide with an unstable equilibrium and disappear in a saddle-node bifurcation, and another that causes a stable equilibrium to become unstable by merging with two unstable equilibria in a pitchfork bifurcation. While both mechanisms lead to snap-through transitions, the dynamics of the transition depends on the type of bifurcation. Saddle-node bifurcation results in algebraic growth of the instability while subcritical pitchfork bifurcation results in exponential growth.[11,12]

Symmetries and symmetry-breaking help explain the force hysteresis observed in Ref. 10 and reproduced in our numerical and analytical models in Fig. 2 and in Ref. 11, Supplemental document. Also, when combined with the normal form analysis, symmetries can be exploited to develop diagnostic tools for predicting the type of shape transition the system undergoes and to anticipate when the system is approaching a bifurcation and even to predict the exact position of the bifurcation point μ^* when it is not known a priori.[11,12]

Importantly, this intuitive yet universal understanding of elastic instabilities based on symmetries of the Euler-buckled strip provides powerful tools for diagnostics and design of elastic transitions. They can help design programmable metamaterials with tunable bistability and rapid (algebraic or exponential) actuation capabilities. For example, for a buckled elastic strip, clamped at both ends and driven via antisymmetric rotations, to undergo a non-linear snap-through, we must break the U-twin symmetry. This can be achieved by using a strip with geometric or material heterogeneity, such as a geometrically-tapered strip instead of a homogeneous strip.[11]

These elastic systems open up new avenues for (i) understanding how biological systems integrate physics with sensing and control to achieve biological function, and (ii) developing new engineering solutions for physically intelligent systems, such as new metamaterials composed of elementary bistable units, that can sense, actuate, and learn.[17]

1) Y. Forterre, J. M. Skotheim, J. Dumais, and L. Mahadevan, Nature **433**, 421 (2005).
2) A. Pandey, D. E. Moulton, D. Vella, and D. P. Holmes, Europhys. Lett. **105**, 24001 (2014).
3) Y. Wang, Q. Wang, M. Liu, Y. Qin, L. Cheng, O. Bolmin, M. Alleyne, A. Wissa, R. H. Baughman, D. Vella, and S. Tawfick, Proc. Natl. Acad. Sci. U.S.A. **120**, e2210651120 (2023).
4) A. Rafsanjani, A. Akbarzadeh, and D. Pasini, Adv. Mater. **27**, 5931 (2015).
5) H. Yasuda and J. Yang, Phys. Rev. Lett. **114**, 185502 (2015).
6) G. Librandi, E. Tubaldi, and K. Bertoldi, Nat. Commun. **12**, 3454 (2021).
7) F. Ling, H. Guo, and E. Kanso, J. R. Soc. Interface **15**, 20180594 (2018).
8) Y. Man and E. Kanso, Soft Matter **15**, 5163 (2019).
9) M. Gomez, D. E. Moulton, and D. Vella, Nat. Phys. **13**, 142 (2017).
10) T. G. Sano and H. Wada, Phys. Rev. E **97**, 013002 (2018).
11) B. Radisson and E. Kanso, Phys. Rev. Lett. **130**, 236102 (2023).
12) B. Radisson and E. Kanso, Phys. Rev. E **107**, 065001 (2023).
13) A. Goriely and M. Tabor, Nonlinear Dyn. **21**, 101 (2000).
14) Y. Man and E. Kanso, Phys. Rev. Lett. **125**, 148101 (2020).
15) M. I. Younis, H. M. Ouakad, F. M. Alsaleem, R. Miles, and W. Cui, J. Microelectromech. Syst. **19**, 647 (2010).
16) S. H. Strogatz, *Nonlinear Dynamics and Chaos with Student Solutions Manual: With Applications to Physics, Biology, Chemistry, and Engineering* (CRC Press, Boca Raton, FL, 1994).
17) H. Yasuda, P. R. Buskohl, A. Gillman, T. D. Murphey, S. Stepney, R. A. Vaia, and J. R. Raney, Nature **598**, 39 (2021).

Basile Radisson obtained a Ph.D. at the University of Aix-Marseille in 2019. He was a postdoctoral researcher at the University of Southern California in Professor Eva Kanso's lab from 2019 to 2022. He now holds a postdoctoral position at Université Libre de Bruxelles in Brussels, Belgium. His research focuses on the fundamental understanding of mechanical instability phenomena in fluids and solids with the aim of harnessing their dynamics in engineering and biological applications.

Eva Kanso is a professor and the Z. H. Kaprielian Fellow of Aerospace and Mechanical Engineering at the University of Southern California (USC). Kanso is on rotation as a Program Director the National Science Foundation since Fall 2021. Prior to joining USC in 2005, Kanso held a two-year postdoctoral position in Computing and Mathematical Sciences at Caltech. She received a Ph.D. degree in 2003 and an M.S. degree in 1999 in Mechanical Engineering, as well as an M.A. degree in 2002 in Mathematics, all from the University of California at Berkeley. She obtained her Bachelor of Engineering degree from the American University of Beirut with distinction. Kanso's research interests concern fundamental problems in the biophysics of cellular and subcellular processes and the physics of animal behavior, both at the individual and collective levels. A central theme in her work is the role of the mechanical environment, specifically the fluid medium and fluid-structure interactions, in shaping and driving biological functions.